

Practical Induction Heating Coil Designs for Clinical Hyperthermia with Ferromagnetic Implants

P. R. Stauffer, *Member, IEEE*, P. K. Sneed, H. Hashemi, *Member, IEEE*, and T. L. Phillips

Abstract—Interstitial techniques for hyperthermia therapy of cancer continue to evolve in response to requirements for better localization and control over heating of deep seated tissues. Magnetic induction heating of ferromagnetic implants is one of several available techniques for producing interstitial hyperthermia, using thermal conduction to redistribute heat within an array of controlled temperature “hot sources.” This report describes seven induction heating coil designs that can be used for producing strong magnetic fields around ferromagnetic seed implants located in different sites in the body. The effect of coil design on the extent and uniformity of the magnetic field is characterized, and appropriate electrostatic shield designs for minimizing electric field coupling to the patient are described. Advantages and disadvantages of each coil type are discussed in terms of the radiated fields, coil efficiency, and ease of use, and appropriate applications are given for each design. This armamentarium of induction coils provides the ability to customize magnetic field distributions for improved coupling of energy into ferromagnetic implant arrays located at any depth or orientation in the body. Proper selection of heating coil configuration should simplify patient setup, improve the safety of patient treatments, and pave the way for future applications of interstitial heating in sites that were previously untreatable.

Index Terms—Hyperthermia, ferromagnetic implant, induction coils, coil design, solenoids, surface coils.

I. INTRODUCTION

THREE interstitial heating modalities are currently under investigation for use in hyperthermia therapy of cancer: radiofrequency electrodes, implantable microwave antennas, and “hot source” techniques [1]. While initial development focused primarily on the first two techniques (due to their ability to deposit power directly in tissue at distance from the implanted sources), considerable attention has shifted in recent years to the development of fundamentally simpler hot source technologies that have potentially more controllable and predictable heating patterns in heterogeneous tissue [2], [3]. Several thermal conduction-based interstitial heating techniques are being pursued, including hot water tubes [4], [5], DC voltage powered resistance wires [6]–[8], and ferromagnetic implants with either catheter born sources [9]–[12] or colloidal suspensions of “magnetic fluids” [13], [14]. Although each of these techniques heats tissue by simple transfer of

thermal energy away from the heated implant surface, there are significant differences in the clinical methodologies of use, flexibility of control over the temperature distributions, and potential clinical applications.

Most clinical studies of ferromagnetic implant hyperthermia have used tumor-length strings of ferromagnetic seeds or stranded wire implants that are afterloaded into an array of plastic catheters, before and after the brachytherapy interval [15]–[20]. Due to the heating equipment size and the requirement to limit electromagnetic radiation to meet federal (FCC) regulations, ferromagnetic implant hyperthermia treatments have been performed in special electromagnetic shield-rooms located in the hyperthermia suite, while the multi-day brachytherapy is given in separate radiation-shielded patient rooms. This type of sequential modality treatment regimen fails to capitalize on the unique characteristics of the Ferroseed heating technique: no requirement for external power connections, and automatic temperature regulation of the implanted thermoseeds. Improvements in the previously reported induction heating system hardware could facilitate alternative clinical protocols [2] that may prove more efficacious: 1) long term continuous heating for 48–72 hours [21]–[23] at temperatures below pain threshold; 2) simultaneous interstitial heat and either interstitial [7] or external beam radiation [24]; and 3) combination thermoradiotherapy sources implanted permanently in the tumor bed to allow repeated heat treatments after surgery [9].

In order to facilitate these clinical approaches, several improvements have been required in the induction heating system hardware, techniques, and implant materials that were used initially. The ongoing development of thermoregulating ferromagnetic implant materials has been reported elsewhere [25]–[29]. Work on 2-D and 3-D algorithms for treatment planning, with thermal conduction-only heat sources, has also progressed rapidly [6], [8], [30]–[34]. The current effort addresses changes in the induction heating coil hardware used to generate the external magnetic field around the ferromagnetic implant. The following sections describe the evolution of coil design, from large inefficient coils with relatively homogeneous magnetic field distributions covering entire regions of the body, to more compact, portable heating coils that conform closely to the body surface. Coil modifications, such as field canceling windings and electrostatic shields that further improve heating efficiency and reduce electromagnetic emissions, are described. Magnetic field distributions are characterized for each coil, and recommendations are given for the appropriate clinical uses of each design.

Manuscript received April 16, 1992; revised August 3, 1993. This work was supported in part by NIC grants R23-CA39428, R01-CA39468, and a gift from Mr. Clarence Heller.

P. R. Stauffer, P. K. Sneed, and T. L. Phillips are with the Radiation Oncology Dept. at the University of California, San Francisco, CA 94143-0226.

H. Hashemi is with Apple Computer, Cupertino, CA.
IEEE Log Number 9213863.

TABLE I
INDUCTION HEATING COIL CONSTRUCTION AND PERFORMANCE PARAMETERS

INDUCTION COIL DESIGN	FIGURE REF. (#)	# OF TURNS (#)	OUTSIDE DIAMETER (cm)	INSIDE DIAMETER (cm)	AXIAL LENGTH (cm)	EFFECTIVE TREATMENT ZONE ¹			COIL POWER@ Ho = 900A/m(W)	COIL FILL FACTOR ² (Ratio)
						DIAMETER (cm)	LENGTH (cm)	VOLUME (cc)		
CONCENTRIC COILS										
Double Layer Solenoid	1b	10	80	66	28	47	44	76,300	730	0.54
Multilayer Spiral Sheet	1c	7	97	64	5	42	40	55,400	1750	1.5
Concentric Oval Solenoid	2b	8	57 × 72	41 × 57	23	31 × 43	46	49,500	415	0.66
SURFACE COILS										
Double Layer Solenoid	1b	12	71	50	19	32	15	12,100	485	0.16
Planar Spiral 'Pancake'	-	13	28	13	2	10	5	400	75	0.32
Transverse Axis Coil Pair	1d	12 each	91	51	10 each	64	107	289,500	2470	0.74
Conformal Surface Coil	1e	7	33 × 22	27 × 16	2.5	27 × 16	12	4,500	315	3.03

¹For concentric coils, the Effective Treatment Zone is calculated as the volume of tissue in a field strength between $\pm 33\%$ of the field at the coil center (H_0) so that $H_{max} \leq 2 H_{min}$. For surface coils, the Effective Treatment Zone represents the tissue region within 50% of the field at the coil-tissue interface, so that again $H_{max} \leq 2 H_{min}$ in tissue.

² Coil Fill Factor is the ratio of the volume having a magnetic field $\geq 50\% H_{max}$ to the volume defined by the boundaries of the coil windings.

II. MATERIALS AND METHODS

All induction heating coils were constructed using dehydrated annealed soft-copper refrigeration tubing for the electrical windings. The spiral sheet coil used 0.030-inch thick annealed copper sheet material for the coil turns. A continuous length of copper tubing was soldered along the centerline of the sheet, to facilitate circulation of water coolant and to provide electrical connection to the matching circuit. In order to maintain the high electrical conductivity of the pre-annealed copper metal, the coils were formed with a minimum of cold working. The interchangeable coils were connected to the matching network components with 0.5-inch diameter copper tubing, with Swagelok 316 Stainless Steel tubing connectors. Spacing between coil turns was maintained either with strips of low density Styrofoam, or with Tygon tubing equivalent in diameter to the copper tubing turns. All coils had a minimum of one 0.5-inch thick layer of low density Styrofoam, both inside and outside the coil turns, for insulation and mechanical support of the coil structure. The Styrofoam sheets were secured by wrapping the entire coil with 2-inch wide cloth tape. Completed coils were coated with epoxy resin for a durable, easy to clean finish. Dimensions of the specific coils characterized in this work are listed in Table I.

A. Concentric Coils

A schematic drawing of a basic solenoid coil is shown in Fig. 1(a), with a depiction of the associated electric (E) and magnetic (H) field orientations. This well-known coil configuration has been described in numerous textbooks and is mentioned here as the starting point for more complex designs. To reduce the externally radiated field relative to the treatment field inside the coil, the solenoid structure was modified by adding a second layer of turns wound back in the opposite direction over top of the first layer [Fig. 1(b)]. This *Double Layer, Reverse Wound Solenoid* was constructed around a cylindrical form, consisting of a 1-inch-thick layer of low density Styrofoam separating the two layers of copper

tubing turns. The spacing between individual turns of each layer was maintained with 0.5-inch-wide strips of Styrofoam. Two such double layer solenoids were constructed: an 80-cm diameter 10 turn coil and a 71-cm diameter 12-turn coil.

In order to fit concentrically around the human torso, solenoids with very large diameters were required. To minimize overall coil size while maintaining sufficient extra room for moving large non-ambulatory patients in and out, the *Concentric Oval Solenoid* was formed by squashing a round solenoid coil into the more appropriate oval shape. The 0.5-inch thick layers of Styrofoam, taped firmly to the inside and outside of the solenoid coil turns, aided in producing a uniform oval shape without kinking the thin wall copper tubing turns.

The *Multilayer Spiral Sheet Coil* design diagrammed in Fig. 1(c) allowed a further increase in the number of coil turns possible within a short axial length, while at the same time eliminating the undesirable axially directed electric field. For this coil, the turns were wrapped one above the other in a progressively increasing diameter spiral. The coil resistance was reduced by using a 5-cm-wide strip of copper sheet material for the turns, rather than wire or tubing with less surface area. Variation of this 5-cm axial coil length provided a means of adjusting the heating coil quality factor (wL/R), power efficiency, and field distribution within the coil. To allow use at high power levels, adequate cooling of the thermally insulated copper sheet turns was obtained by soldering a single 0.375-inch diameter copper tube to the center of the sheet before rolling up the spiral, and subsequently circulating water coolant through the tubing. The spiral sheet coil was constructed with 7 turns, increasing in diameter from a 64 cm aperture to an outer diameter of 97 cm.

B. Transverse Axis Surface Coils

A large *Transverse Axis Coil Pair* configuration was constructed to couple energy into ferromagnetic implants oriented across the body axis. The magnetic field from such a system is shown conceptually in Fig. 1(d). To generate sufficient field

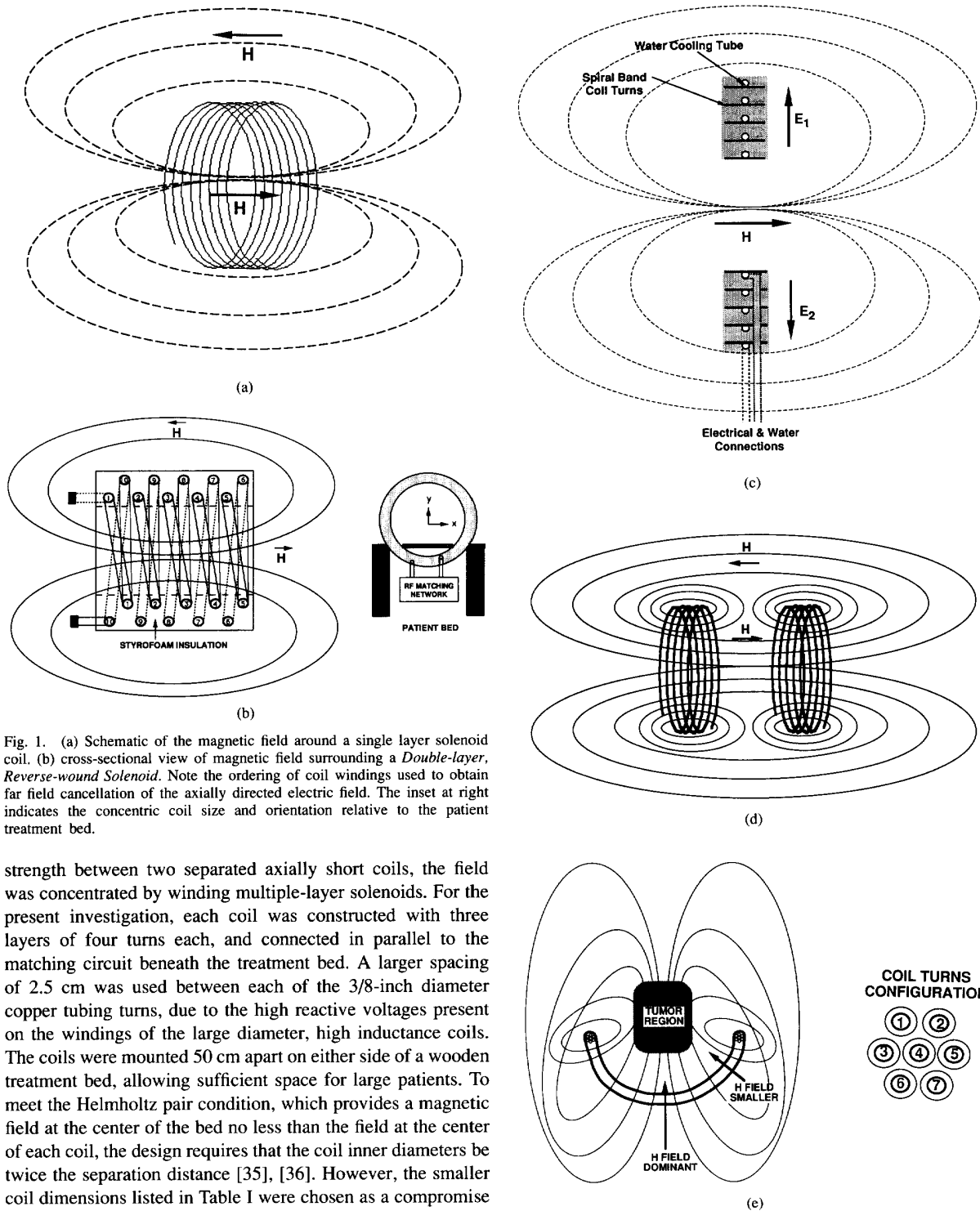


Fig. 1. (a) Schematic of the magnetic field around a single layer solenoid coil. (b) cross-sectional view of magnetic field surrounding a *Double-layer, Reverse-wound Solenoid*. Note the ordering of coil windings used to obtain far field cancellation of the axially directed electric field. The inset at right indicates the concentric coil size and orientation relative to the patient treatment bed.

strength between two separated axially short coils, the field was concentrated by winding multiple-layer solenoids. For the present investigation, each coil was constructed with three layers of four turns each, and connected in parallel to the matching circuit beneath the treatment bed. A larger spacing of 2.5 cm was used between each of the 3/8-inch diameter copper tubing turns, due to the high reactive voltages present on the windings of the large diameter, high inductance coils. The coils were mounted 50 cm apart on either side of a wooden treatment bed, allowing sufficient space for large patients. To meet the Helmholtz pair condition, which provides a magnetic field at the center of the bed no less than the field at the center of each coil, the design requires that the coil inner diameters be twice the separation distance [35], [36]. However, the smaller coil dimensions listed in Table I were chosen as a compromise to limit system size, because maintaining a uniform field across the entire bed was not crucial for activating thermally self-regulating implants located in only a small portion of the field.

A *Planar Spiral Pancake Coil* was constructed in two tightly packed layers by winding 13 turns of 3/16-inch diameter copper tubing in a spiral out from a central opening of 13

Fig. 1. (continued) (c) cross-section of a *Multilayer Spiral Sheet Coil* with copper tubing for electrical and water connections soldered to the rolled up 5-cm wide copper strip. (d) Magnetic field distribution surrounding two coaxially mounted solenoid coils—the *Transverse Axis Coil Pair*. (e) Magnetic field distribution surrounding a saddle-shaped *Conformal Surface Coil* in the intended position around a tumor volume. The relative position of coil windings shown in the inset minimizes the potential difference between turns.

cm. Electrical insulation and spacing of the coil turns was obtained by first encasing the copper tubing in 1/4-inch inside diameter Tygon tubing having a wall thickness of 3/32 inch. The windings of the resulting thin planar "pancake" coil had inner and outer diameters of 13 cm and 28 cm, respectively, and an axial thickness of 2 cm. As in the other coils, distilled, deionized water was circulated through the copper tubing to cool the coil.

The planar spiral coil was modified as shown in Fig. 1(e) to produce a field perpendicular to the body axis, that could extend further in front of the coil face. This *Conformal Surface Coil* was formed by winding 7 turns of 3/16" copper tubing into a 30 cm diameter coil with closely spaced turns at the outer circumference and a large central opening. The coil turns were encased in 1/4-inch inner diameter, 3/32-inch wall Tygon tubing for electrical isolation and control of spacing. The circular winding scheme shown in the inset of Fig. 1(e) was used to minimize the radiated field by far field cancellation of oppositely directed electric field components. This winding scheme also assured that no more than 3/7 of the total coil potential difference existed between any two adjacent windings, to maximize coil turn density without high voltage breakdown. After pressing the multi-turn coil into an oval shape, the coil was further reshaped by bending the two short sides of the oval out of the coil back plane to form two elevated "wings." To solidify the geometry, the multi-turn coil was encased in a single 1-inch diameter Tygon tube slit down one side for access, and finish-coated with a layer of epoxy. The completed Conformal Surface Coil consisted of a 33 × 22 cm oval cross-section with side wings extending up 18 cm from the coil back plane.

C. Electrostatic Shield Designs

Two electrostatic shield designs were built and tested in answer to the need for reducing strong electric field components within the heating coil aperture. The shields were used to minimize direct tissue heating [37], [38] and capacitive coupling of high potentials to the essentially grounded patient within the coil [39]. The simplest shield compatible with the above described heating coils is shown in Fig. 2(a). The metallic strips were mounted perpendicular to the coil windings, with distinct gaps between strips to minimize magnetic field induced eddy currents in the conductors and consequent perturbation of the coil's magnetic field. The complete wire cage design, shown mounted around an oval shaped solenoid in Fig. 2(b), was built to improve the shielding of near-field radiation, both inside and outside the coil. The most critical aspect of this second shield design was the interconnection of fine wires to each other and to an electrical grounding point. A high density of wires (one #22 gauge copper wire per cm of outer circumference) was used to establish a virtual ground plane around the treatment coil. In order to connect all wires to ground, a strap was run around the coil, concentric with the coil turns. To avoid magnetic field (transformer) coupling into this ground strap and to minimize asymmetric deterioration of the heating coil field, the open circuited strap was extended just less than one complete loop and was located

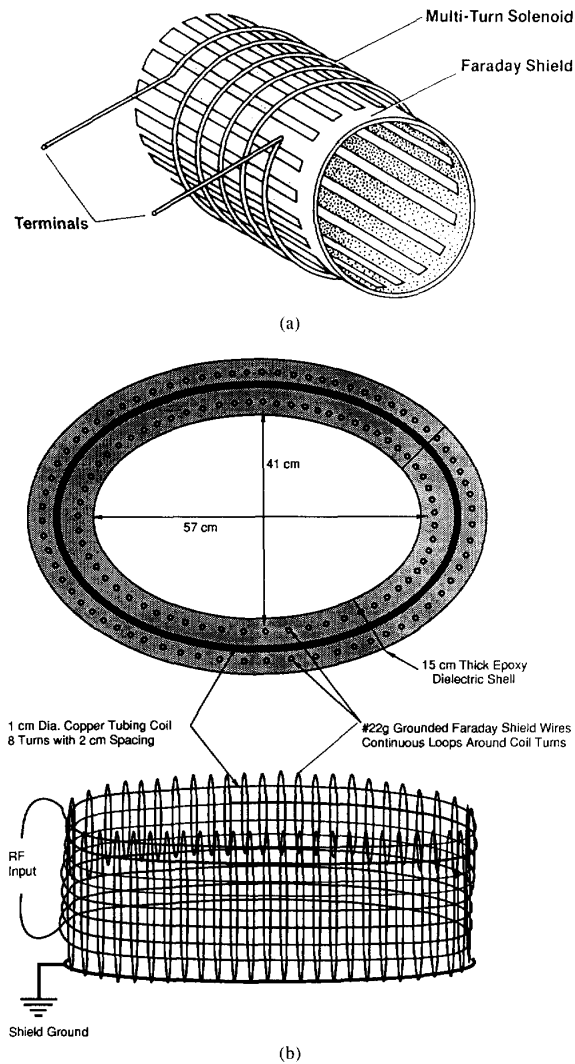


Fig. 2. (a) Sketch of a comb-shaped electrostatic shield mounted inside a single layer solenoid. The air gap between metal strips minimizes eddy current losses from magnetic field coupling to the shield, while the conducting strips short out the axially directed electric field. The shield is separated from the coil turns by two flexible layers of 0.5-inch thick Styrofoam sheets, to minimize capacitive coupling. Figure adapted from [40]. (b) Sketch of the *Concentric Oval Solenoid* cross-section showing the centrally located coil turns encased in Styrofoam and epoxy coating. The coil turns are surrounded by an array of parallel wire loops spaced 1 cm apart around the coil perimeter. The #22 gauge wire loops are each soldered to a single 3/16-inch diameter copper tubing ground strap that is located off one end of the coil, 10 cm beyond the last coil turn.

as far outside the coil turns as possible (10 cm axially beyond the last coil turn). In addition, the grounded wires were spaced radially away from the coil windings by a distance sufficient to minimize capacitive coupling to the shield. For the present application with maximum voltages of 10–15 kV at 100 KHz, adequate spacing and electrical isolation of the shield wires from the coil turns was accomplished with two 0.5 inch thick layers of intervening Styrofoam. Due to the proximity of metallic conductors to the heating

coil turns, some coupling of energy into the shield wires and grounding strap was unavoidable. Because the coils were encased in electrically and thermally insulating Styrofoam, the non-negligible amount of heat (resulting from induced currents in the shield) was removed by circulating cooled water through the circumferential grounding strap.

D. Induction Heating System

Coils were driven with an ENI 9600 EGR generator at 100 ± 5 Hz. The amplifier supplied up to 8 KW of power into a series resonant, transformer-coupled, double-tuned matching circuit similar to that described previously [40]. Heating coil connections to the large tuning capacitors (40–65 nF, 18 kV_{rms}) were made with 0.5-inch diameter annealed copper refrigeration tubing that has very high electrical and thermal conductivities. During operation of the system, temperature-regulated water at 15 °C was circulated through the heating coil and all matching circuit connections carrying high current, including the air core transformer that provided isolation and impedance transformation into the low current primary. The heating coils were mounted on a wooden treatment bed in the center of a 9' x 12' x 7'6" electromagnetic shieldroom enclosure.

E. Evaluation of Heating Coil Performance

Magnetic Field Measurements To characterize magnetic field distributions around the heating coils, a magnetic field meter was constructed following the design of Oleson [41] and Gross [42]. A single-axis magnetic field sensor was constructed by winding 10 turns of #40 gauge wire around a 2.5-cm diameter form that contained a light emitting diode, photodetector, and temperature compensation circuit. The probe was connected to the remote readout electronics by a fiberoptic link that was minimally perturbing to the heating-coil field. The meter was calibrated to read in absolute magnetic field strength using a 5-cm diameter, 35-cm long calibration solenoid. This long thin solenoid had 312 tightly packed turns to generate a homogeneous directional magnetic field in the center of the solenoid. The calibration field was calculated from the measured coil current and known coil parameters. After calibration, the probe was linear and accurate to better than 5% over a range of 100–2500 A/m. Field maps were generated by manually recording field strengths at 1 or 2.5 cm increments along the following linear tracks: 1) along the coil axis; 2) across the central coil diameter; 3) across the coil front face; and 4) parallel to the coil front face but at various axial distances from the coil. A non-metallic linear positioning device with a spatial precision of 5 mm was used for mapping all linear field profiles. Contour plots of the magnetic field distributions were generated from regularly spaced linear profiles of field strength in one cross-sectional plane of the coil using the DissplaTM graphics package from Integrated Software Systems Corp. (San Diego). No data smoothing or averaging routines were used which would alter the raw contour data.

Analysis of Field Distributions Magnetic field distributions around the induction coils were described in terms of the

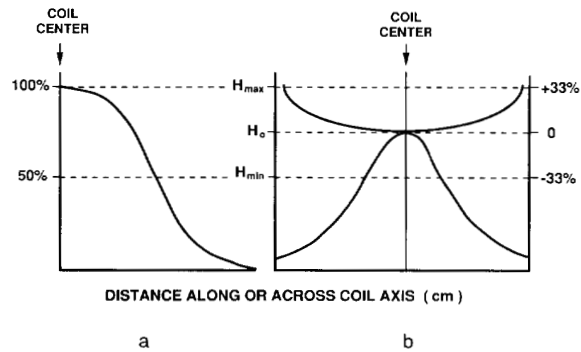


Fig. 3. Diagram of typical magnetic field distributions showing the interrelationship of H_{min} , H_o (at coil center), and H_{max} : (a) field profile along the coil central axis to one side of a surface coil; (b) field profiles along the coil central axis (bottom), and laterally across the coil diameter at the axial coil center (top).

percentage of maximum field strength (H_{max}) within the coil. In order to compare the relative performance of quite different heating coil configurations, an arbitrary criterion of acceptable magnetic field uniformity was established. For this analysis, an “acceptable” field for inductive coupling into an array of ferromagnetic implants was defined such that the minimum field (H_{min}) within the intended implant volume was at least 50% of the maximum field (H_{max}) anywhere in the tissue load (i.e., $H_{max} \leq 2H_{min}$). For surface coils placed next to the skin surface, the 100 KHz magnetic field falls off essentially monotonically into tissue from its maximum at the skin/coil interface. Thus an “Effective Treatment Zone” was identified for surface coils as the volume off to one side of the coil having a field strength of at least 50% of the surface value H_{max} . The field surrounding a coil placed concentrically around the load is more complex. It falls off in either direction axially from the peak (H_o) at coil center, and increases above H_o for increasing radial distances approaching the coil turns. Thus, for concentric coils, the “Effective Treatment Zone” was identified as the volume inside and around each coil having a field strength range of $H_o \pm 33\%$. As shown diagrammatically in Fig. 3, the $H_{max} \leq 2H_{min}$ criterion defining the Effective Treatment Zone is represented equivalently for the two differently shaped fields by ranges of field strength from 50%–100% H_{max} , or by $H_o \pm 33\%$.

Coil Efficiency The relative power efficiency of the different coils was quantified by two methods: 1) by measuring the power level required for each coil to produce a field strength of 900 A/m at a common reference point along the coil axis; and 2) by recording the reference point field strength as a function of applied power to the coil. For concentric coils, the reference point was the central axis peak near coil center (H_o). For surface coils, the measurement point was the central axis peak at the coil/tissue interface (H_{max}). The reference point for the transverse axis coil pair was taken midway between coils along the common axis. In order to quantify the relative ability of different coil configurations to produce large effective treatment fields with minimum coil size, another

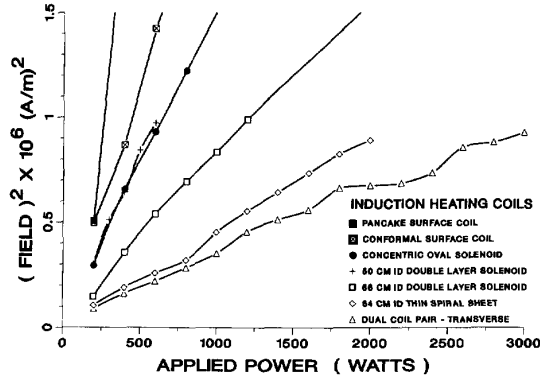


Fig. 4. Coil center magnetic field squared versus applied power. The lower curves obtained with the larger heating coil configurations indicate poorer efficiency, but all coils show that applied power is directly proportional to the resultant field squared.

measure of coil efficiency was identified as the "Coil Fill Factor." This performance measure was calculated as the ratio of "Effective Treatment Zone" volume to the volume defined by the boundaries of the coil windings.

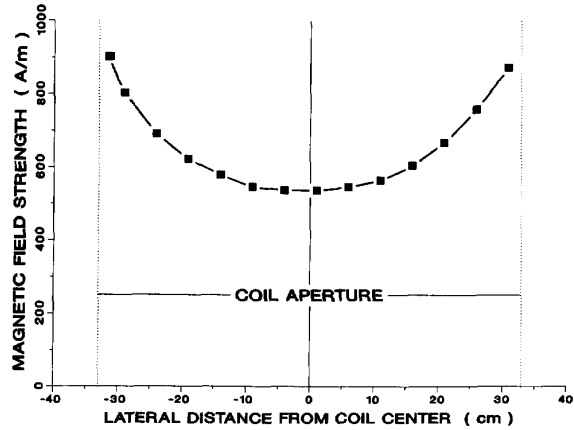
III. RESULTS

Magnetic field performance measures for each of the coil designs are summarized in Table I. Relative power efficiencies for the different coil designs are listed in the table and are also presented graphically in Fig. 4, which demonstrates the variation in reference point magnetic field strength as a function of applied power. Applied power was directly proportional to the square of the resultant magnetic field in all coils except for approximately a 10% deterioration of field strength at high power levels in the large transverse axis coil pair.

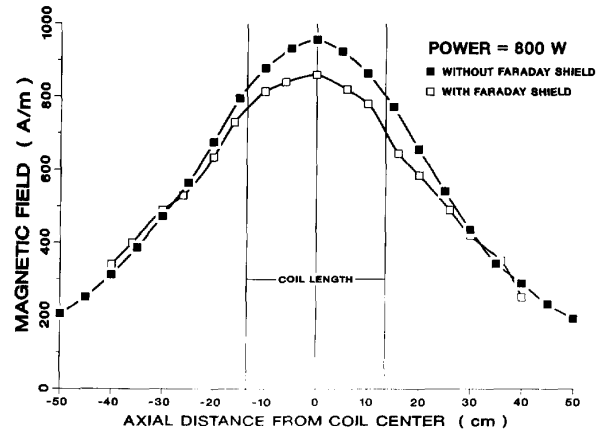
A. Concentric Coils

Fig. 5(a) shows the magnetic field strength measured across the central diameter of the 28-cm long, 66-cm inside diameter *Double Layer, Reverse Wound Solenoid*. For this large concentric body coil, the magnetic field is within 33% of the value at coil center ($H \leq 1.33H_0$) for a distance of 47 cm across the coil interior. As shown in Fig. 5(b), the Effective Treatment Zone of this coil (where H is between $H_0 \pm 33\%$) extended 44 cm along the coil axis, or 8 cm outside the coil boundaries in both directions. The roughly cylindrical volume of tissue within $\pm 33\%$ of the field at coil center was 76,300 cm³. Fig. 5(b) also demonstrates the magnetic-field perturbation effects of an interior-only electrostatic shield, which reduced the coil's central axis magnetic field by at most 10% near coil center. The power required to produce a field of 900 A/m at the center of this concentric body coil was 730 W.

The effect of bending a round solenoid into an oval shape that better fits the human torso is shown in Fig. 6. The magnetic field profiles, plotted laterally across the central diameter and across the coil front face, demonstrate the field deterioration which results from significantly distorting a 46-cm long, 53-cm inner diameter round coil into a 41 ×



(a)



(b)

Fig. 5. (a) Magnetic field distribution laterally across the central diameter of a 66-cm inner diameter, 28-cm long *Double-layer, Reverse-wound Solenoid*. Power = 200 W. (b) Magnetic field distribution along the central axis of a *Double-layer, Reverse-wound Solenoid*, with and without an interior-only electrostatic shield of the design shown in Fig. 2a. Power = 800 W.

57-cm oval shape. The effect of adding a complete fine-wire electrostatic shield cage, such as that shown in Fig. 2(b), is also shown in Fig. 6. For this smaller, electrostatically shielded *Concentric Oval Solenoid* that more appropriately fits the shape of the torso, the effective treatment zone was still 49,000 cm³. The power level required to obtain the reference field of 900 A/m at coil center was 315 W.

The lateral field profile across the central diameter of the *Multilayer Spiral Sheet Coil* is given in Fig. 7(a). Fig. 7(b) gives the field along the coil axis. The region within $\pm 33\%$ of the central coil magnetic field extended 17.5 cm outside the coil boundaries in both directions along the central axis and 42 cm across the coil interior, for a total Effective Treatment Zone of 55,400 cm³. The power required to provide a field of 900 A/m at coil center was 1750 W.

B. Transverse Axis Surface Coils

Fig. 8 shows the magnetic field oriented normal to the tissue surface off to one side of a 19-cm long, 71-cm outer diameter

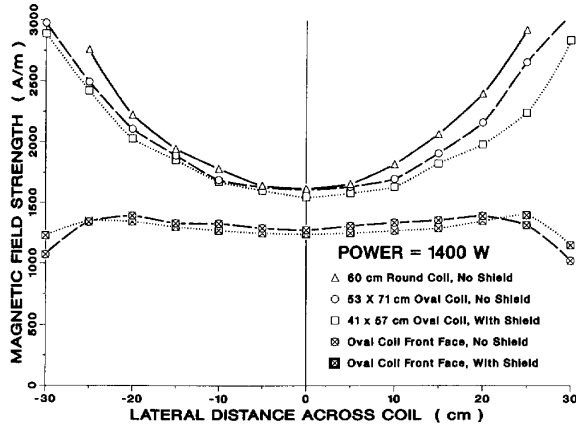


Fig. 6. Composite plot of magnetic field distributions measured laterally across the central diameter (upper 3 curves), and across the coil front face (lower curves) of an unshielded 23-cm long, 60-cm inner-diameter round single-layer solenoid that was subsequently formed into a 52 x 71 cm oval coil, and shielded with the metal cage shield of Fig. 2(b). Magnetic field measurements are given before and after installation of the electric field shielding.

Double Layer, Reverse Wound Solenoid coil intended for use adjacent to (rather than concentric with) the implant. The field strength fell to 50% of its coil front face value at a distance of 15 cm from the coil, producing an Effective Treatment Zone of 12,100 cm³. For a smaller 28-cm diameter, 13-cm inner diameter *Planar Spiral ‘Pancake’ Coil* that would be more appropriately sized for coupling to the body surface, the field dropped to 50% of its surface strength at a depth of only 5 cm (Fig. 9). This produced an Effective Treatment Zone of 400 cm³ but required a power level of only 75 W to produce the reference field of 900 A/m at the tissue surface.

Fig. 10 demonstrates the expansion of Effective Treatment Zone possible using a *Transverse Axis Coil Pair*. For this arrangement of two 91-cm diameter, 51-cm inner diameter and 10-cm long solenoid coils spaced 50 cm apart center to center, the field varied less than ± 33% over a region extending 90 cm across the axis of the bed and 64 cm vertically and axially along the bed. This coil pair configuration produced a region of relatively uniform magnetic field over 289,530 cm³ of tissue. The power required to produce a field strength of 900 A/m at the centrally located reference point was 2470 W.

Fig. 11(a) shows the magnetic field distribution in the central cross-sectional plane of the much smaller *Conformal Surface Coil*. The amount of magnetic field asymmetry due to the non-planar coil geometry is quantified in Fig. 11(b). The field profile along the coil axis showed that the region ≥50% H_{max} extended 12.3 cm along the axis between coil wings but only 3.9 cm to the back side of the coil. The Effective Treatment Zone of the field oriented perpendicular to the body axis (and perpendicular to the coil back plane) was 4, 500 cm³. The angular dependence of power deposition from this irregularly shaped omnidirectional coil field into a 6-cm long #430 stainless steel implant, centered in the Effective Treatment Zone, is quantified in Fig. 12. The power required to produce the 900 A/m field strength at the tissue surface reference point was 315 W. Because of the compact nature of

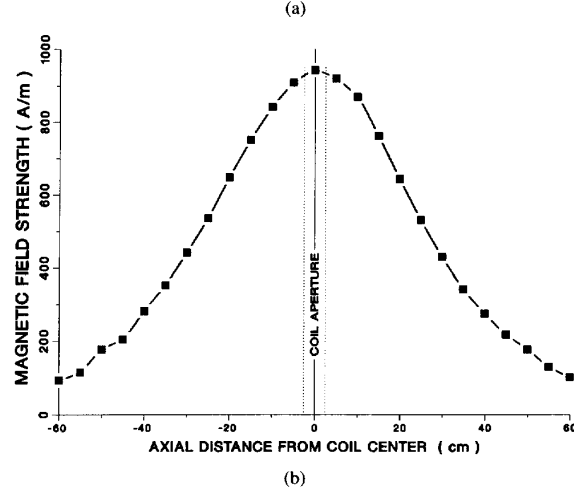
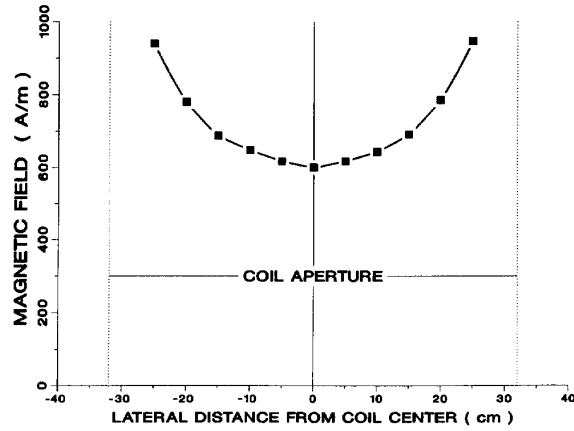


Fig. 7. (a) Magnetic field profile across the central diameter of a 5-cm long, 50-cm inner diameter *Multilayer Spiral Sheet Coil*. Note similarities to the Fig. 5(a) solenoid field. Power = 500 W. (b) Magnetic field along the *Spiral Sheet Coil* central axis. Note similarities to Fig. 5b, though the field was generated from a considerably shorter length coil. Power = 2000 W.

this tightly wound body-conforming coil, the Coil Fill Factor of 3.0 was the highest of all coils tested.

IV. DISCUSSION AND CONCLUSION

Initially, all induction heating coils were intended to produce large regions of uniform magnetic field, to reduce the positioning dependence of a patient in the coil required for equal power deposition in all ferromagnetic implants of an array [10], [12]. A region of relatively uniform field that is larger than the tumor dimensions may be obtained quite easily with coils that are axially long compared to the tumor dimensions, as well as large enough in diameter to fit concentrically around the human torso. This is clear from the concentric coil-field distributions of Figs. 5–7 and from the Coil Fill Factors listed in Table I, which demonstrate that all concentric coils tested produce a relatively uniform field distribution over at least 54% of the coil volume—considerably larger than the implant volume in every case. Because cylindrically shaped ferromagnetic implant materials must be aligned within approximately 30° of the magnetic field to absorb energy

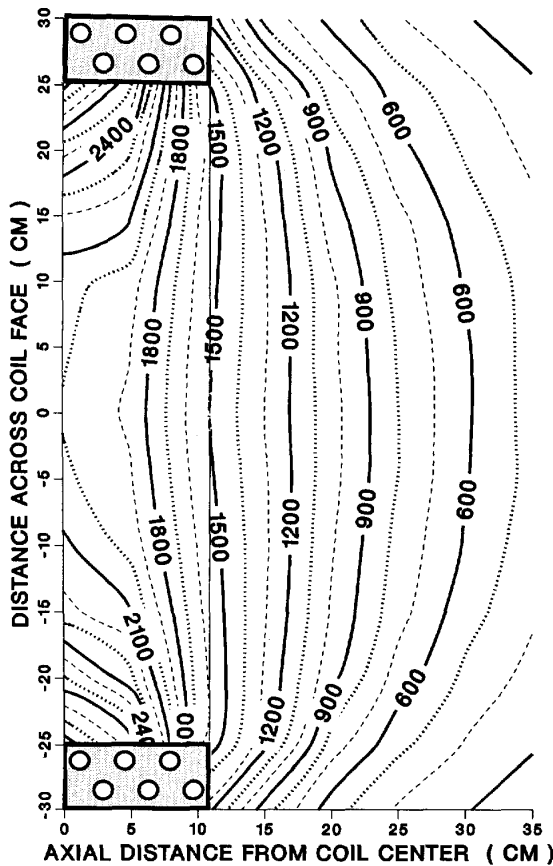


Fig. 8. Axially directed magnetic field surrounding a 50-cm inner diameter round Solenoid intended for use as a surface coil. The field falls to 50% of its value at the coil front face ($z = 11$ cm) at an axial distance of 15 cm from the coil. Power = 3000 W.

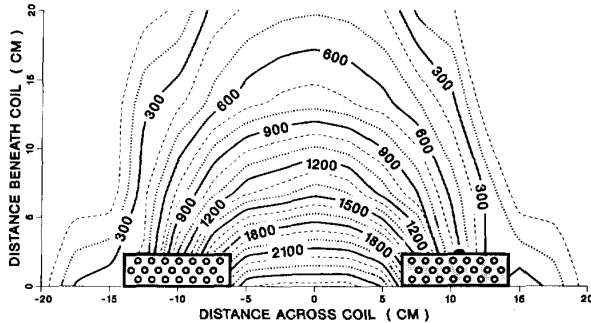
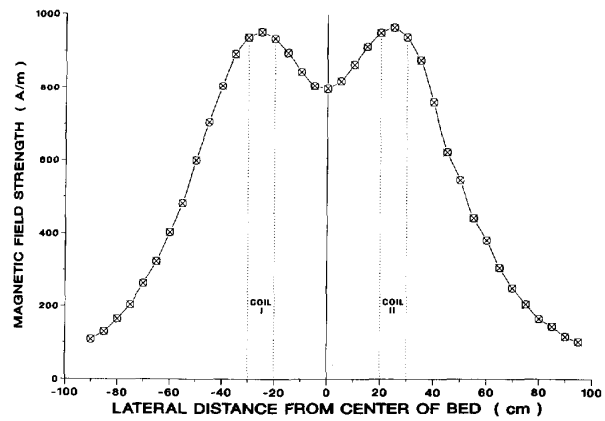
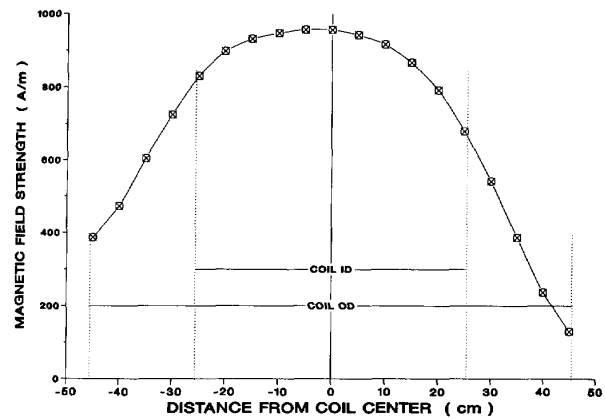


Fig. 9. Magnetic field in front of a 13-cm inner diameter Planar Spiral Pancake Coil, showing a relatively small volume of tissue contained in the effective treatment zone from 50-100% H_{max} . Power = 400 W.

efficiently [9], [16], [33], and because many tumors are not amenable to surgical implantation of catheters along the body axis, concentric coils which produce fields along the body axis are not always desirable. Often a magnetic field oriented across the body axis is preferable. As demonstrated in this paper, reasonably uniform magnetic field distributions over large volumes may still be achieved using a number of different coil configurations. For ferromagnetic implants consisting of Curie



(a)



(b)

Fig. 10. (a) Magnetic field profile across the bed along the central axis of the Transverse Axis Coil Pair with two 51-cm inner diameter, 91-cm outer diameter coils driven in parallel at 100 KHz. Note the large region of relatively uniform magnetic field. Power=1600 W. (b) Magnetic field along the bed axis, centered between the two transverse-mounted coils. Power = 2400 W.

Point alloys with reasonably good self-thermoregulation [12], [27]–[29], [43], the variation of implant temperature within the target volume should be acceptably small for magnetic field variations less than a factor of 2 or 3 [1], [33]. This paper describes several practical heating coil designs that can be used for producing magnetic fields with this level of uniformity around Ferroseed arrays implanted either parallel or perpendicular to the long axis of the body.

The Solenoid is a particularly versatile induction heating coil design. This basic structure produces large regions of relatively uniform field within the coil and has been used successfully in a number of ferromagnetic seed heating systems [10], [12], [26], [28], [44]. For a solenoid, the magnetic field strength is directly proportional to the number of coil turns and coil current. To reduce the current (and system power) for a given field strength, the number of turns within the same axial-coil length may be increased. The associated increase in coil inductance produces higher voltage across the coil and tuning capacitor components. Thus, electrostatic shielding of the coil windings becomes increasingly important, to reduce potentially hazardous reactive voltages located close to the

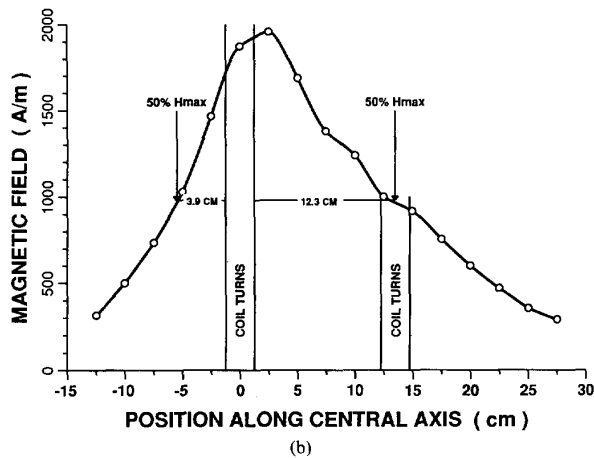
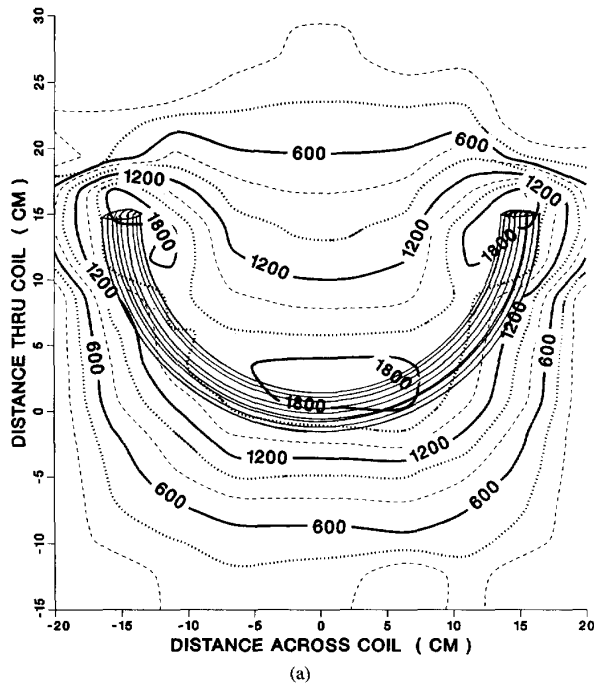


Fig. 11. (a) Cross-section of the magnetic field distribution around the *Conformal Surface Coil*. Power = 800 Watts. (b) Magnetic field profile along the central axis of the *Conformal Surface Coil*. Note the extended penetration of the field between coil wings relative to the field off the back of the coil. Power = 800 Watts.

patient and treatment personnel. Further increases in power efficiency may be obtained by concentrating the magnetic field with multiple layer coils having higher axial winding density. If the turns are wound in opposing directions in the different layers, such as the *Double Layer, Reverse Wound Solenoid* tested in this work, a reduction of the externally radiated field may result due to cancellation of electric field vectors. The need for electrostatic shielding to reduce the intense near field becomes even more pronounced with this coil design, however, due to the higher potentials between adjacent turns.

Regardless of winding density or number of layers, all solenoids produce an axially directed magnetic field inside

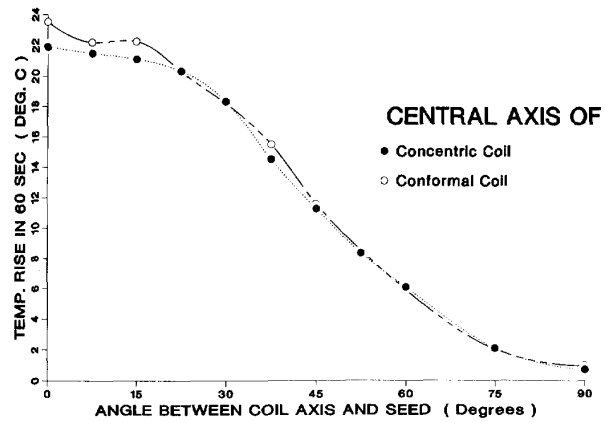


Fig. 12. Variation of heating power with angle between a 6-cm long, 17 gauge, #430 stainless steel needle in a calorimeter cell and the central axis of two heating coils. The calorimeter cell was placed in regions of equivalent field strength at the center of the Effective Treatment Zone of a round *Solenoid* and between the coil wings of the *Conformal Surface Coil* (at position $x = 0$, $y = 8$ cm in Fig. 11(a)).

the coil that falls off rapidly away from the coil front face, as shown in Figures 5(b) and 8. For activation of implanted ferromagnetic seed materials, these coils are used most effectively when placed concentrically around the implant, to produce large regions of relatively uniform magnetic field oriented along the body axis. The major drawbacks of this treatment configuration are: 1) ferromagnetic implants must be aligned with the body axis, which frequently is an inconvenient surgical approach; 2) there are difficulties associated with moving non-ambulatory patients into a confining coil aperture; and 3) the large coils necessary for encompassing the human torso may produce excessive radiated energy (proportional to the field strength and coil area). Coupling of the magnetic field to the implant array may be improved by conforming the coil shape to the body contour around the implant and reducing the coil cross-section for a closer fit. The *Concentric Oval Solenoid* sketched in Fig. 2(b) is one example of a coil optimized for coupling energy into implants oriented along the axis of the human torso. As seen in Fig. 6, there is very little effect on the magnetic field homogeneity near coil center when a round solenoid is modified to this more appropriate oval shape. For ferromagnetic seeds implanted normal to the tissue surface, solenoid coils placed perpendicular to the body surface may be useful as surface coils if coil diameters much larger than the depth and lateral extent of the required magnetic field region are used. While usable fields ($\geq 50\% H_{max}$) may be generated as far as 15 cm in front of large diameter solenoids (Fig. 8), coupling the large coils to the patient surface is generally awkward and results in substantially increased leakage fields that do not couple the implant.

Concentration of the magnetic field within an axially short aperture is possible using a large diameter *Multilayer Spiral Sheet Coil*. This configuration has very little axially directed electric field but produces a significant radial electric-field component next to the coil turns, which must be shielded for use close to the operator and patient. The field distribution across the coil interior is similar to that of single- and

multilayer solenoids, but extends further along the axis outside the coil. For example, the coil center field (H_o) for the 66-cm inner diameter, 28-cm long double layer solenoid is 61% of the peak field (H_{max}) near the coil turns [Fig. 5(a)]. This is directly comparable to the $64\%H_{max}$ field obtained centrally in the 64 cm inner diameter, multilayer spiral coil that is only 5 cm long [Fig. 7(a)]. The axial length having a field $\geq 67\%$ of H_o extends along the coil axis 8 times the length of the spiral coil however, rather than just 1.5 times the solenoid coil length. As the axial length of the spiral sheet is increased significantly beyond this 5 cm prototype, the current density increases noticeably towards the axial ends of the coil and decreases centrally. Practical configurations for the spiral sheet design range from the axially short coil characterized in Fig. 7, to the axially long coil reported previously [10]. Because of the very large diameter of the outermost coil turns, the multilayered spiral has a much larger region of high field (both radially and axially) than a solenoid of equivalent inner diameter. Because of this larger storage field, the spiral coils have significantly poorer coupling to the tissue volume, and hence lower power efficiency. Thus the multilayer spiral may be best suited for applications requiring large regional magnetic fields—perhaps oriented normal to the tissue surface off to one side of the coil.

For large or deep-seated implant arrays requiring large volumes of uniform magnetic field oriented perpendicular to the body axis, the *Transverse Axis Coil Pair* configuration shown schematically in Fig. 1(d) may be required. This configuration produces a quite uniform magnetic field distribution over a large region between coils (Fig. 10), but is consequently electrically inefficient (Fig. 4) and extremely high in leakage radiation to the surrounding environment. Future transverse axis, dual-coil systems would likely benefit from the use of multilayer spiral sheet coils due to their extended axial field distribution, though poor power efficiency would continue to be a concern. Nonetheless, this dual coil configuration may be the system of choice for activating long implants located deep in the body and oriented across the body axis.

Perhaps more convenient for many applications requiring a field perpendicular to the body surface is the *Planar Spiral "Pancake" Coil* configuration. These coils are easily made small enough to fit conveniently against the skin surface, but produce correspondingly smaller regions of usable magnetic field. The strong magnetic field immediately adjacent to the coil windings falls off rapidly with both axial distance in front of the coil face and radial position in front of the coil (Fig. 9). Power-limiting radially directed electric fields near the closely spaced coil turns further restrict the effective penetration depth of the magnetic field, since energy is coupled directly into the adjacent tissue [45]. The proper use and limitations of planar pancake coils for applications in direct heating of superficial tissues at frequencies above 10 MHz has been described previously [45], [46]. At 100 kHz, the planar coils may be useful for coupling energy into small ferromagnetic implant arrays oriented across the body axis and located close to the tissue surface in relatively flat anatomical regions. This might include superficial implants in the trunk and extremities.

The present effort introduces a new coil design that is a modification of the planar pancake coil; one which can be used

to project the magnetic field deeper into the patient in regions where the coil can be wrapped around the body contour. The magnetic field of this *Conformal Surface Coil* is shown, in Fig. 11, to penetrate 12.3 cm into the tissue in the "saddle" of the coil. This is significantly deeper field penetration than that obtained with a planar pancake coil (Fig. 9) of similar diameter. The conformal surface coil configuration appears most appropriate for implant arrays oriented vertically or laterally across the body axis in the head and neck, breast, or extremities. If the coil is wrapped about the perineum anterior to posterior, like a saddle, the coil may also prove useful for energizing pelvic implants oriented along the body axis. In fact, such coils may be preferable for this application due to the simplicity of patient coupling, compared to physically loading non-ambulatory patients into the confining aperture of a concentric coil. In contrast to the large diameter concentric coils, there is no central region of homogeneous uni-directional magnetic field, however. Instead, there is a region of steadily decreasing field adjacent to the coil. Thus, this type of coil relies more heavily on Ferroseed self-thermoregulation to obtain equal temperatures, in spite of the field gradient along the implant length. For a typical pelvic implant consisting of 7-cm long Ferroseeds located 7-14 cm deep to the perineum, the field adjacent to the conformal surface coil would range from 950-1500 A/m along the implant length, at a power level of 800 Watts (Fig. 11). Existing Curie point Ferroseeds should have sufficient thermoregulation to produce nearly equal temperatures when driven with this range of field strengths [1], [33]. The corresponding maximum field of 2000 A/m at the coil/tissue interface is sufficiently low that direct heating of surface tissues in the 100 kHz field would be entirely negligible compared to tissue heating around the implants.

Another potential concern for the *Conformal Surface Coil* is the more complex multidirectional field pictured in Fig. 1(e), which results from non-planar geometry of the coil windings. The critical function of the induction coil for Ferroseed heating applications is not to produce a high-quality directional field, but to produce magnetic field coupling into ferromagnetic implants that may or may not be entirely parallel. Field coupling is quantified as implant power absorption in Fig. 12, for the worst case of a non-thermoregulating, small-diameter cylindrical implant. The data demonstrate that magnetic coupling into a 6-cm long, #17 gauge needle is relatively constant for angles within about 30° of the axis of the coil back plane. Although power absorption is seen to fall off dramatically for implants oriented greater than 30° off axis, this is almost identical to the angular dependence of seed heating obtained in large-diameter, axially short solenoids, as shown in this work (Fig. 12) and elsewhere [9], [16], [33]. Thus, the non-homogenous magnetic field does not appear to have a significant effect on the power absorption characteristics of cylindrical implants located within the Effective Treatment Zone of the *Conformal Surface Coil*.

An interior-only electrostatic shield design, such as that shown in Fig. 2(a), was used successfully with early solenoid heating coils to reduce electric field coupling to the patient's skin [10] and surrounding environment [39]. Subsequent coil designs with more complex coil-winding schemes and orienta-

tions to the body axis have required more complete shielding, however. The fine wire shield cage introduced in this work [Fig. 2(b)] accomplishes two major goals. It shorts out a significant portion of the intense electric fields generated between coil turns, without a significant effect on magnetic field coupling to the adjacent tissues (Figs. 5–6). This allows the essentially grounded patient and treatment personnel to touch the coil-housing surface without fear of arcing from high potentials on the coil windings. Additionally, the extra layers of electrical insulation around the shielding cage increase the thickness of the coil housing, so the patient's skin is held further away from the sharply higher magnetic fields near the coil turns. In practice, this shield design has been effective at eliminating all electric-field coupling hazards, such as electrostatic discharge from either the patient's skin or coil surface to any partially grounded object (i.e., treatment personnel, IV pole, etc.). Fine wire grounding cages, such as that shown in Fig. 2(b), may be equally effective when applied to multilayer solenoids, spiral-sheet coils, or non-planar conformal-surface coil designs. While a quantitative study of electric field distributions surrounding the heating coils was not possible in the present research, this will be investigated in future efforts to produce coils that can be used safely outside an electromagnetic shieldroom. The final step, of making high-efficiency, well-shielded coils that meet FCC regulations on radiated emissions, should increase the number of applications for ferromagnetic-seed heating by allowing new treatment protocols which use portable systems for long-term heating in the patients's radiation-shielded room or near linear accelerators in the radiotherapy clinic.

In summary, several heating coil designs were described that can be used for producing strong magnetic fields around ferromagnetic implants located either superficially or deep in the body, and oriented either along or perpendicular to the body axis. The rationale and construction details for electrostatic shields that minimize electric field coupling between the coil, patient, and operating personnel were described. The effect of coil design on the extent and uniformity of magnetic field distributions was characterized. Finally, the advantages and disadvantages of each coil type were discussed in terms of treatment and leakage fields, coil power efficiency, and ease of use in the clinic. Recommendations were made for appropriate clinical applications of each design.

ACKNOWLEDGMENT

The authors would like to acknowledge the extremely helpful comments, suggestions, and continual motivation from Dr. Thomas Cetas of the University of Arizona. We also acknowledge the efforts of Mike Hodges, Andrew Tomlinson, and Dr. Dayton Misfeldt of Thermea, Inc., whose collaboration helped in the evolution of the Conformal Surface Coil design.

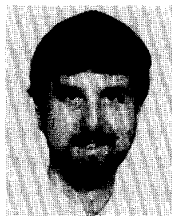
REFERENCES

- [1] P. R. Stauffer, "Techniques for interstitial hyperthermia," in *An Introduction to the Practical Aspects of Clinical Hyperthermia*, J. Hand and S. Field, Eds., New York: Taylor and Francis, 1990, pp. 344–370.
- [2] P. R. Stauffer, "Interstitial Hyperthermia—Evolving Technologies," in *Proc. of Radiation Research: A 20th Century Perspective*, vol. 2, J.

- D. Chapman, W. C. Dewey and G. G. Whitmore, Eds., Toronto: Academic Press, 1991, pp. 906–911.
- [3] J. W. Strohbehn and J. A. Mechling, "Interstitial techniques for clinical hyperthermia," in *Physical Techniques in Clinical Hyperthermia*, J. W. Hand and J. R. James, Eds., New York: John Wiley & Sons, 1986, pp. 210–287.
- [4] J. W. Hand, B. S. Tremblay, and M. V. Prior, "Physics of Interstitial hyperthermia: radiofrequency and hot water tube techniques," in *Hyperthermia and Oncology Vol. 3: Interstitial Hyperthermia*, M. Urano and E. Double, Eds. Zeist: VSP, 1989.
- [5] K. Schreier, M. Budihna, H. Lesnicar, L. Handl-Zeller, J. W. Hand, M. V. Prior, S. T. Clegg, and I. A. Brezovich, "Preliminary studies of interstitial hyperthermia using hot water," *Int. J. Hyp.*, vol. 6, no. 2, pp. 431–444, 1990.
- [6] C. F. Babbs, N. E. Fearnot, J. A. Marchosky, C. J. Moran, J. T. Jones, and T. D. Plantenga, "Theoretical basis for controlling minimal tumor temperature during interstitial conductive heat therapy," *IEEE Trans. BME*, vol. 37, no. 7, pp. 662–672, 1990.
- [7] J. A. Marchosky, D. M. Welsh, and C. J. Moran, "Hyperthermia treatment of brain tumors," *Missouri Med.*, pp. 29–33, January, 1990.
- [8] J. A. DeFord, C. F. Babbs, U. H. Patel, N. E. Fearnot, J. A. Marchosky, and C. J. Moran, "Accuracy and precision of computer-simulated tissue temperatures in individual human intracranial tumors treated with interstitial hyperthermia," *Int. J. Hyp.*, vol. 6, no. 4, pp. 755–770, 1990.
- [9] C. V. Burton, J. M. Mozley, A. E. Walker, and H. E. Braitman, "Induction thermocoagulation of the brain: A new neurosurgical tool," *IEEE Trans. BME*, vol. 13, no. 3, pp. 114–120, 1966.
- [10] P. R. Stauffer, A. M. Fletcher, D. W. DeYoung, M. W. Dewhurst, J. R. Oleson, and T. C. Cetas, "Observations on the use of ferromagnetic implants for inducing hyperthermia," *IEEE Trans. BME*, vol. 31, no. 1, pp. 76–90, 1984.
- [11] W. J. Atkinson, I. A. Brezovich, and D. P. Chakraborty, "Usable frequencies in hyperthermia with thermal seeds," *IEEE Trans. BME*, vol. 31, no. 1, pp. 70–75, 1984.
- [12] I. A. Brezovich, W. J. Atkinson, and D. P. Chakraborty, "Temperature distributions in tumor models heated by self-regulating nickel-copper alloy thermoseeds," *Med. Phys.*, vol. 11, pp. 145–152, 1984.
- [13] R. W. Rand, H. D. Snow, D. G. Elliot, and M. Snyder, "Thermomagnetic surgery for cancer," *Applied Biochemistry and Biotechnology*, vol. 6, pp. 265–272, 1981.
- [14] A. Jordan, P. Wust, H. Fahling, W. John, A. Hinz and R. Felix, "Inductive heating of ferrimagnetic particles and magnetic fluids: physical evaluation of their potential for hyperthermia," *Int. J. Hyp.*, vol. 9, no. 1, pp. 51–68, 1993.
- [15] R. G. Heath, S. B. John, and C. J. Fontana, "Stereotaxic implantation of electrodes in the human brain: A method for long-term study and treatment," *IEEE Trans. BME*, vol. 23, no. 4, pp. 296–304, 1976.
- [16] A. E. Walker and C. V. Burton, "Radiofrequency telethermocoagulation," *J. Am. Med. Assoc.*, vol. 197, no. 9, pp. 108–112, 1966.
- [17] D. Stea, D. Shimm, J. Kittelson, and T. C. Cetas, "Interstitial hyperthermia with ferromagnetic seed implants: Preliminary results of a Phase I clinical trial," in *Interstitial Hyperthermia*, L. Handl-Zeller, Ed., New York: Springer-Verlag, 1992, pp. 183–193.
- [18] B. Seta, J. Kittelson, J.R. Cassady, A. Hamilton, A. N. Guthkelch, B. Lulu, E. Obbens, K. Rossman, W. Shapiro, A. Shetter, and T. C. Cetas, "Treatment of malignant gliomas with interstitial irradiation and hyperthermia," *Int. J. Radiat. Oncol. Biol. Phys.*, vol. 34, pp. 657–667, 1992.
- [19] K. Au, T. C. Cetas, D. Shimm, J. Chen, R. Sinno, S. Haider, D. Buechler, W. Lutz, and R. J. Cassady, "Interstitial ferromagnetic hyperthermia and brachytherapy; preliminary results of a phase I clinical trial," *Endocurie.Hyp. Oncol.*, vol. 5, pp. 127–136, 1989.
- [20] C. F. Mack, B. Stea, J. M. Kittelson, D. S. Shimm, P. K. Sneed, T. L. Phillips, P. S. Swift, K. Luk, P. R. Stauffer, K. W. Chan, R. Steeves, J. R. Cassady, and T. C. Cetas, "Interstitial thermoradiotherapy with ferromagnetic implants for locally advanced and recurrent neoplasms," *Int. J. Radiat. Oncol. Biol. Phys.*, vol. 27, pp. 109–115, 1993.
- [21] E. Armour, Z. Wang, P. Corry, and A. Martinez, "Equivalence of continuous and pulse simulated low dose rate irradiation in 9L gliosarcoma cells at 37° and 41°," *Int. J. Radiat. Oncol. Biol. Phys.*, vol. 22, pp. 109–114, 1991.
- [22] P. M. Corry, A. Martinez, E. P. Armour and G. Edmundson, "Remote afterloading: State of the art," in *Proc. of Brachytherapy Meeting*, Dearborn, MI, 1989, pp. 193–204.
- [23] J. A. Marchosky, C. F. Babbs, C. J. Moran, N. E. Fearnot, J. A. DeFord, and D. M. Welsh, "Conductive, interstitial hyperthermia: A new modality for treatment of intracranial tumors," in *Consensus on Hyperthermia for the 1990s*, H.I.Bicher, et al., Eds., New York:

- Plenum Press, 1990, pp. 129-143.
- [24] T. Inoue, N. Masaki, S. Ozeki, H. Ikeda, and T. Kozuka, "Experiences with interstitial hyperthermia as a sole treatment modality or combined with radiotherapy," in *Interventional Radiation Therapy: Techniques-Brachytherapy*, R. Sauer, Ed., New York: Springer Verlag, 1991, pp. 371-374.
- [25] C. V. Burton, M. Hill, and A. E. Walker, "The RF thermoseed: A thermally self-regulating implant for the production of brain lesions," *IEEE Trans. BME*, vol. 18, pp. 104-109, 1971.
- [26] R. A. Moidel, S. K. Wolfson, R. G. Selker, and S. B. Weiner, "Materials for selective tissue heating in a radiofrequency electromagnetic field for the combined chemothermal treatment of brain tumors," *J. Biomat. Res.*, vol. 10, pp. 327-334, 1976.
- [27] L. J. Demer, J. S. Chen, D. N. Buechler, M. A. Damento, D. R. Poirier, and T. C. Cetas, "Ferromagnetic thermoseed materials for tumor hyperthermia," in *Proc. of IEEE Engr. in Med. and Biol. Society Meeting*, vol. 2, G. V. Kondraske and C. J. Robinson, Eds., Fort Worth: IEEE Press, 1986, pp. 1148-1153.
- [28] T. Kobayashi, Y. Kida, T. Tanaka, N. Kageyama, H. Kobayashi, and Y. Amemiya, "Magnetic induction hyperthermia for brain tumor using ferromagnetic implant with low Curie temperature," *J. Neuro-Onc.*, vol. 4, pp. 175-181, 1986.
- [29] J. S. Chen, D. R. Poirier, M. A. Damento, L. J. Demer, F. Biencaniello, and T. C. Cetas, "Development of NI-4 Wt. Percent Si thermoseeds for hyperthermia cancer treatment," *J. Biomat. Res.*, vol. 22, pp. 303-319, 1988.
- [30] A. Y. Matlobieh, R. B. Roemer, and T. C. Cetas, "Numerical simulation of magnetic induction heating of tumors with ferromagnetic seeds implants," *IEEE Trans. BME*, vol. 31, no. 2, pp. 227-235, 1984.
- [31] Z. P. Chen, W. H. Miller, R. B. Roemer and T. C. Cetas, "Three dimensional computer simulation program for hyperthermia treatment planning," *Int. J. Hyp.*, vol. 6, no. 1, pp. 175-191, 1990.
- [32] R. B. Chin and P. R. Stauffer, "Treatment planning for ferromagnetic seed heating," *Int. J. Radiat. Oncol. Biol. Phys.*, vol. 21, pp. 431-439, 1991.
- [33] S. A. Haider, T. C. Cetas, J. R. Wait, and J. S. Chen, "Power absorption in ferromagnetic implants from radio frequency magnetic fields and the problem of optimization," *IEEE Trans. MTT*, vol. 39, no. 11, pp. 1817-1827, 1991.
- [34] S. A. Haider, T. C. Cetas, and R. B. Roemer, "Temperature distribution in tissue from a regular array of hot source implants: an analytical approximation," vol. 40, no. 5, pp. 408-417, 1993.
- [35] K. Kaminishi and S. Nawata, "Practical method of improving the uniformity of magnetic fields generated by single and double Helmholtz coils," *Rev. Sci. Instrum.*, vol. 52, no. 3, pp. 447-453, 1981.
- [36] J. Oleson, T. Cetas, and P. Corry, "Hyperthermia by magnetic induction: Experimental and theoretical results for coaxial coil pairs," *Rad. Res.*, vol. 95, pp. 175-186, 1983.
- [37] F. S. Chute and F. E. Vermeulen, "A visual demonstration of the electric field of a coil carrying a time-varying current," *IEEE Trans. Ed.*, vol. 24, pp. 278-283, 1981.
- [38] P. S. Ruggera and G. Kantor, "Development of a family of RF helical coil applicators which produce transversely uniform, axially distributed heating in cylindrical fat-muscle phantoms," *IEEE Trans. BME*, vol. 31, pp. 98-106, 1984.
- [39] P. R. Stauffer and J. M. Hevezi, "Possible hazards of patient anaesthesia during hyperthermia therapy," *Int. J. Radiat. Oncol. Biol. Phys.*, vol. 8, pp. 1077, 1982.
- [40] P. R. Stauffer, T. C. Cetas, and R. C. Jones, "Magnetic induction heating of ferromagnetic implants for inducing localized hyperthermia in deep seated tumors," *IEEE Trans. BME*, vol. 31, no. 2, pp. 235-251, 1984.
- [41] J. R. Oleson, "An accurate probe for mapping strong HF magnetic fields," *IEEE Trans. BME*, vol. 29, pp. 581-583, 1982.
- [42] E. Gross, "Optical magnetic field probe with light emitting diode sensor," *M. S. Thesis, Univ. of Arizona, Dept. of Electrical and Computer Engineering.*, 1986.
- [43] R. Deshmukh, M. Damento, L. Demer, K. Forsyth, D. DeYoung, M. Dewhirst, and T. C. Cetas, "Ferromagnetic alloys with curie temperatures near 50°C for use in hyperthermic therapy," in *Proc. of 4th Intl. Symposium on Hyperthermic Oncology 1984*, J. Overgaard, Ed., Aarhus, Denmark: Taylor and Francis, 1984, pp. 599-602.
- [44] J. A. Malloy, R. C. Ritter, W. C. Broadus, M. S. Grady, M. A. Howard III, E. G. Quate, and G. T. Gillies, "Thermodynamics of movable inductively heated seeds for the treatment of brain tumors," *Med. Phys.*, vol. 18, no. 4, pp. 794-803, 1991.

- [45] A. W. Guy, J. F. Lehmann, and J. B. Stonebridge, "Therapeutic Applications of Electromagnetic Power," *Proc. IEEE*, vol. 62, no. 1, pp. 55-75, 1974.
- [46] G. M. Hahn, P. Kernahan, A. Martinez, D. Pounds, S. Prionas, T. Anderson, and G. Justice, "Some heat transfer problems associated with heating by ultrasound, microwaves, or radiofrequency," *Ann. NYAS*, vol. 335, pp. 327-346, 1980.



Paul R. Stauffer (M '81) received the B.A. degree in physics from the College of Wooster, OH, in 1975 and the M.S. degree in electrical engineering from the University of Arizona at Tucson in 1979.

Additional specialization in clinical engineering led him to a position as Research Associate in the Division of Radiation Oncology at the University of Arizona from 1979-1983.

Mr. Stauffer is presently board certified in clinical engineering and medical physics, and is an Associate Professor in the Department of Radiation Oncology at the University of California, San Francisco, where he is Director of Physics and Engineering for Hyperthermia. His current research interests include the development and testing of RF, microwave, and ultrasound hyperthermia applications for more uniform heat distribution to superficial and deep-lying tumors.



Penny K. Sneed received the B.S.E.E. degree summa cum laude at the University of Missouri, Columbia, in 1976 and the M.D. degree from Stanford University in 1981.

Her residency training in radiation oncology was at the University of California, San Francisco, and she spent one year as a postdoctoral fellow investigating brain hyperthermia. Dr. Sneed is currently an Assistant Professor in the Department of Radiation Oncology at the University of California, San Francisco.

Dr. Sneed's areas of interest include hyperthermia, brain brachytherapy, and radiosurgery. She is a "Councilor of Medicine" of the North American Hyperthermia Society and an editorial board member of the *International Journal of Hyperthermia*.

Homayoon Hashemi (M '89) received the B.S. degree in engineering from California State University, Chico, in 1980. After working in the nuclear industry for 3 years, he returned to the University of California, Berkeley and received the M.S. degree in system controls in 1988.

Mr. Hashemi worked as a Graduate Research Assistant in the Hyperthermia Section of the Radiation Oncology Department at the University of California, San Francisco, from 1987-88. Since then he has worked in the fields of software engineering and process control systems, and he is currently working for Apple Computer in Cupertino, CA.



Theodore L. Phillips received the B.S. degree from Dickinson College in 1955, and received the M.D. degree from the University of Pennsylvania in 1959.

He joined the Department of Radiation Oncology at the University of California, San Francisco, in 1963. He has served as Professor and Chairman of the Department of Radiation Oncology at the University of California, San Francisco, since 1978. He is involved with new technological applications for radiation therapy of cancer, including hyperthermia.

Dr. Phillips is the President of the North American Hyperthermia Society, and his current research interests include interstitial techniques for hyperthermia therapy and hyperthermia interactions with radiation and chemotherapy.